LAWRENCE
LIVERMORE
NATIONAL
LABORATORY

LLNL-CONF-405682

Determining the Uncertainty on the Total Heavy Flavor Cross Section

R. Vogt

July 24, 2008

3rd International Conference on Hard and Electromagnetic Probes of High-Energy Nuclear Collisions
Illa de A Toxa, Spain
June 8, 2008 through June 14, 2008

Disclaimer

EPJ manuscript No.
(will be inserted by the editor)

Determining the Uncertainty on the Total Heavy Flavor Cross Section

R. Vogt[1,2]

[1] Lawrence Livermore National Laboratory, Livermore, CA 94551, USA
[2] Physics Department, University of California, Davis, CA 95616, USA

Received: date / Revised version: date

Abstract. We assess the theoretical uncertainties on the total heavy quark cross section. We discuss the importance of the quark mass, the scale choice, the number of light flavors and the parton densities on the estimate of the uncertainty. At first glance, the uncertainty bands on the total charm cross sections obtained by integrating the FONLL inclusive cross section and by integrating the partonic total cross sections appear to be incompatible. We explain how this apparent difference arises and describe how the two results can be reconciled. The small charm quark mass amplifies the effect of varying the other parameters in the calculation, making the uncertainty on the total charm cross section difficult to quantify. On the other hand, the bottom quark total cross section is under much better theoretical control and differences between the two approaches are small.

PACS. 12.38.Bx Perturbative calculations – 14.65.-q Quarks

1 Introduction

Heavy flavor production is rather unique in that the total heavy flavor production cross section is analytically calculable to leading order at the partonic level. In addition the finite heavy flavor mass provides a scale to control the transverse momentum distributions down to $p_T \to 0$. It is thus not only interesting to determine the inclusive kinematic distributions of the heavy flavor production cross section but to also obtain the total cross section as another means of comparing the production cross sections as a function of energy.

Heavy flavor production has been studied using a variety of final-state observables from single leptons and neutrinos in beam-dump experiments to direct reconstruction of heavy flavor hadrons using vertex detectors. The measurements cover a limited region of phase space, making it necessary to extrapolate over the unmeasured region to obtain the total cross section. Before the kinematic dependence of the cross section was under good theoretical control, these extrapolations were of limited utility. Leptonic observables obscure the identity of the parent hadron as well as its momenta while only a limited number of decay channels can be directly reconstructed, typically those into two or three charged hadrons. When the parent hadron can be reconstructed, the branching ratio for the measured decay channel must be known precisely enough to accurately determine the parent hadron production cross section. Thus a number of assumptions are necessary to obtain the total cross section from data including the decay branching ratio; the phase space extrapolation; and correction for the unmeasured hadrons, *e.g.* if only neutral D mesons are measured, the non-observation of the charged D mesons, the D_s and the charm baryons must be corrected for.

No previous measurements of the total heavy flavor cross section have been made in pp collisions in the RHIC energy regime. The fixed-target experiments are all at much lower hadron-hadron center-of-mass energy $\sqrt{S}$. The previous total cross section measurements at colliders were from the ISR at $53 \leq \sqrt{S} \leq 63$ GeV. At energies greater than $\sqrt{S} = 200$ GeV, the only total cross section data available are statistics limited: an upper limit from UA1 and some cosmic ray data. While the b total cross section was obtained at the Tevatron in $p\overline{p}$ collisions at $\sqrt{S} = 1.8$ and 1.96 TeV, the charm hadron measurements are only available at $p_T > 5$ GeV, not allowing a realistic extrapolation to $p_T = 0$. A determination of the total heavy flavor cross section at RHIC would show whether or not the RHIC measurements are consistent with other previous data.

While the consistency of the data are important, there is also more than one way to calculate the total cross section using higher-order techniques. The most straightforward method is to calculate the total hadronic cross section directly using the next-to-leading order matrix elements for the total partonic cross section [1],

$$\sigma_{pp}(S,m^2) = \sum_{i,j=q,\overline{q},g} \int dx_1\, dx_2 \times f_i^p(x_1,\mu_F^2)\, f_j^p(x_2,\mu_F^2)\, \widehat{\sigma}_{ij}(s,m^2,\mu_F^2,\mu_R^2) \quad (1)$$

where x_1 and x_2 are the fractional momenta carried by the colliding partons and f_i^p are the proton parton densities[1]. This remains the state of the art for the total cross section; there is still no complete NNLO evaluation of the total cross section, especially at energies where $\sqrt{S} \gg m$. In this case, the mass is the only relevant scale in the calculation since the kinematics of the produced quarks do not enter.

However, when the kinematic distributions are measured, especially at $p_T \gg m$, the state-of-the-art calculation is the fixed-order next-to-leading logarithm approach (FONLL) [2]. In addition to including the full fixed-order NLO result [1,3], the FONLL calculation also resums [4] large perturbative terms proportional to $\alpha_s^n \log^k(p_T/m)$ to all orders with next-to-leading logarithmic (NLL) accuracy (*i.e.* $k = n$, $n-1$). The FONLL calculation treats the heavy quark as an active light flavor at $p_T >> m$. Thus the number of light flavors used to calculate α_s includes the heavy quark, *i.e.* $n_{\rm lf}+1$ where, for charm, $n_{\rm lf} = 3$ (u, d and s). The same number of flavors, $n_{\rm lf}+1$, is also used in the FONLL fixed-order calculation.

If the inclusive electron spectrum from heavy flavor decay is measured, the calculation of the cross section involves three components: the p_T and rapidity distributions of the heavy quark Q, calculated in perturbative QCD; fragmentation of the heavy quarks into heavy hadrons, H_Q, described by phenomenological input extracted from e^+e^- data; and the decay of H_Q into electrons according to spectra available from other measurements, schematically written as

$$\frac{Ed^3\sigma(e)}{dp^3} = \frac{E_Q d^3\sigma(Q)}{dp_Q^3} \otimes D(Q \to H_Q) \otimes f(H_Q \to e) \quad (2)$$

where the symbol $\otimes$ denotes a generic convolution. The electron decay spectrum, $f(H_Q \to e)$, accounts for the semileptonic branching ratios.

The total cross sections obtained by integrating the FONLL kinematic distributions, Eq. (2), should be equivalent to that obtained by convoluting the total partonic cross sections with parton densities, Eq. (1). We discuss the theoretical uncertainty obtained based on Eq. (1) and how that uncertainty compares to the FONLL result [5] obtained by integrating Eq. (2).

In both cases, the perturbative parameters are the heavy quark mass and the value of the strong coupling, α_s, while the parton densities are a nonperturbative input. We take $m_c = 1.5$ GeV and $m_b = 4.75$ GeV as the central values with $1.3 \le m_c \le 1.7$ GeV and $4.5 \le m_b \le 5$ GeV to estimate the mass uncertainties. The perturbative calculation also depends on the unphysical factorization (μ_F) and renormalization (μ_R) scales. (These scale parameters are unphysical in the sense that the real cross section should be independent of the scale.) The sensitivity of the cross section to their variation can be used to estimate the perturbative uncertainty due to the absence of higher orders. Since Eq. (1) is independent of the kinematics, we take $\mu_{R,F} = \mu_0 = m$ as the central value and varied the two scales independently within a 'fiducial' region defined by $\mu_{R,F} = \xi_{R,F}\mu_0$ with $0.5 \le \xi_{R,F} \le 2$ and $0.5 \le \xi_R/\xi_F \le 2$. In practice, we use the following seven sets: $\{(\xi_R,\xi_F)\} = \{$(1,1), (2,2), (0.5,0.5), (1,0.5), (2,1), (0.5,1), (1,2)$\}$. The uncertainties from the mass and scale variations are added in quadrature. The envelope containing the resulting curves,

$$\sigma_{\rm max} = \sigma_{\rm c} + \sqrt{(\sigma_{\mu,\rm max} - \sigma_{\rm c})^2 + (\sigma_{m,\rm max} - \sigma_{\rm c})^2}\ , \quad (3)$$

$$\sigma_{\rm min} = \sigma_{\rm c} - \sqrt{(\sigma_{\mu,\rm min} - \sigma_{\rm c})^2 + (\sigma_{m,\rm min} - \sigma_{\rm c})^2}\ , \quad (4)$$

defines the uncertainty as a function of energy. Here $\sigma_{\rm c}$ is the cross section calculated at the central value, $(\xi_R,\xi_F) = (1,1)$ and $m_c = 1.5$ GeV, $m_b = 4.75$ GeV, while $\sigma_{i,\rm max}$ and $\sigma_{i,\rm min}$ are the maximum and minimum values of the cross section for a given mass ($i = m$) or (ξ_R,ξ_F) set in the fiducial region ($i = \mu$). Although Eqs. (3) and (4) have been written for the total cross section, the corresponding maximum and minimum differential distributions can be written similarly [5].

We will first show the results for the total heavy flavor cross section calculated from the total partonic cross section for charm and bottom. We then discuss the various sources contributing to the uncertainty in the calculation of the total heavy flavor cross section: the parton densities (PDFs), the mass and the scales. We compare our results to those obtained by integrating the FONLL distributions over full phase space.

2 Results

The total partonic cross section is written as

$$\widehat{\sigma}_{ij}(s,m,\mu_F^2,\mu_R^2) = \frac{\alpha_s^2(\mu_R^2)}{m^2}\Bigg\{ f_{ij}^{(0,0)}(\rho) + 4\pi\alpha_s(\mu_R^2)\left[f_{ij}^{(1,0)}(\rho) + f_{ij}^{(1,1)}(\rho)\ln\left(\frac{\mu_F^2}{m^2}\right)\right] + \mathcal{O}(\alpha_s^2)\Bigg\} \quad (5)$$

where $\rho = 4m^2/s$ and $f_{ij}^{(k,l)}$ are the $q\overline{q}$, gg and $(q+\overline{q})g$ scaling functions to NLO [1]. The NNLO $f_{ij}^{(2,l)}$ scaling functions for $ij = gg$ and $q\overline{q}$ have been calculated through expansion of the resummed cross section to next-to-next-to-leading logarithm (NNLL) [6,7] and beyond [8–10]. While the scale dependence is better under control at the next order, the complete NNLO correction is still of the same order as the NLO correction, *e.g.* a factor of two or so [7, 9] for charm, showing that the charm cross section is slow to converge.

At small ρ, the $\mathcal{O}(\alpha_s^2)$ and $\mathcal{O}(\alpha_s^3)$ $q\overline{q}$ and the $\mathcal{O}(\alpha_s^2)$ gg scaling functions become small while the $\mathcal{O}(\alpha_s^3)$ gg and qg scaling functions plateau at finite values [1]. Thus, at collider energies, the total cross sections are primarily dependent on the small x parton densities and phase space.

The total cross section does not depend on the kinematics but only on the quark mass, m, and the renormalization and factorization scales with central value $\mu_{R,F} =$

[1] Note that we use S for the square of the hadronic center-of-mass energy and s for the partonic center-of-mass energy.

m. The heavy quark is always considered massive in the calculation of the total cross section and is thus not an active flavor in the production calculation. Therefore, the number of light quark flavors, $n_{\rm lf}$, does not include the heavy quark so that α_s is calculated with $n_{\rm lf} = 3$ for charm and 4 for bottom.

The theoretical uncertainty on the total cross section is calculated using Eqs. (3) and (4). The energy dependence of the charm and bottom total cross sections is shown in Figs. 1 and 2 respectively. The left-hand sides are calculated with the CTEQ6M PDFs while the right-hand sides are calculated with GRV98 set. The entire range from fixed-target to collider energies are shown. The central value of the band is indicated by the solid curve while the upper and lower edges of the band are given by the dashed curves. The charm results of Ref. [11], calculated with $\mu_F = \mu_R = 2m_c$ and $m_c = 1.2$ GeV, lie well within the CTEQ6M band and near the upper edge of the GRV98 band. Note that the charm uncertainty band broadens as the energy increases. The lower edge of the charm band grows more slowly with $\sqrt{S}$ above RHIC energies while the upper edge is compatible with the reported total cross sections at RHIC [12,13].

The NLO total cross sections at $\sqrt{S} = 200$ GeV and 5.5 TeV are summarized in Table 1. The $\sqrt{S} = 200$ GeV results are compared to the FONLL total cross sections reported in Ref. [5].

We first look at the NLO and FONLL cross sections at $\sqrt{S} = 200$ GeV, both calculated with CTEQ6M. The NLO central values are only about 25% and 10% higher than FONLL for charm and bottom respectively. However, the width of the uncertainty band is larger for the NLO calculation, particularly for charm. The differences in the width of the bottom uncertainty band are much smaller. On the other hand, both the GRV98 central values and corresponding uncertainties are smaller than all results calculated with CTEQ6M at $\sqrt{S} = 200$ GeV.

At 5.5 TeV, the central charm cross section is $2.5 - 3.5$ mb, similar to other calculations. However, the uncertainty is much larger than at the RHIC energy, particularly for the CTEQ6M calculation. Although the central values for bottom production at 5.5 TeV are similar to those for charm at 200 GeV, the uncertainty is much reduced.

In the next section, we will discuss the apparent discrepancy between the FONLL and NLO total cross sections as well as the differences in the CTEQ6M and GRV98 results. We also discuss the various sources of uncertainty to explain why the charm uncertainty is so large.

3 Sources of uncertainty

From the results in Table 1, it appears that the total cross section depends on whether it is calculated from the integral over the inclusive FONLL p_T distribution, Eq. (2) or from the total NLO partonic cross sections, Eq. (1). The difference seems especially large for charm production. This is primarily due to the way the strong coupling constant is calculated and to the low x, low scale behavior of the parton densities.

Here, we discuss these two contributions to the theoretical uncertainty and show that, if the total cross section is calculated the same way, the two results are, in fact, equivalent, as they should be. We also discuss the scale dependence of the cross section.

3.1 Parton densities

Our main results are calculated with the CTEQ6M PDFs, the same ones used in the FONLL calculations of Ref. [5]. The charm calculations are very sensitive to the low x and low μ_F behavior of the parton densities, particularly the gluon density. Probing the full fiducial range of the uncertainty band is problematic for charm production since $\xi_F = 0.5$ is below the minimum scale of the CTEQ6M parton densities, $\mu_0^{\rm CTEQ6M} = 1.3$ GeV [14]. Thus, for $\mu_F = 0.5m_c$, significant backward evolution of the parton densities is required. Most recent PDFs exhibit similar behavior. To probe the PDF dependence more fully, we thus use the GRV98 densities [15] with a lower minimum scale, $\mu_0^{\rm GRV98} = 0.89$ GeV, resulting in faster evolution to higher μ_F. The lower minimum scale requires less backward evolution to reach the factorization scale $\mu_F = 0.5m_c$. The gluon densities at $\mu_F = 0.5m_c$, m_c and $2m_c$ are shown in Fig. 3 for both PDF sets.

At sufficiently high μ_F relative to μ_0, the gluon density increases with decreasing x. While this typical behavior is observed for the GRV98 PDFs with $\mu_F = m_c$ and $2m_c$, it is only seen for the CTEQ6M PDFs for $\mu_F = 2m_c$. The highest low x gluon density is at the largest scale. Note that for $x > 0.1$ the lower scales have higher densities.

At lower scales, the gluon density no longer increases with decreasing x. With the CTEQ6M densities at $\mu_F = m$, the dashed curve on the left-hand side of Fig. 3 is no longer increasing with decreasing x but, instead, is almost flat for $x < 10^{-2}$ with a slight dip in the middle. Lower x values are not shown for $\mu_F = 0.5m_c$ because the backwards evolution gives $xg(x, \mu_F) \leq 0$, accounting for the high $\sqrt{S}$ behavior of the lower bound on the uncertainty band. On the other hand, the GRV98 gluon density is better behaved for $\mu_F = 0.5m$. This is because the GRV98 analysis assumes valence-like gluon densities at their lower initial scale so that while the density flattens it does not become negative. Note also that while the GRV98 densities are somewhat lower than CTEQ6M when $x > 0.01$, they are higher at lower x, accounting for the larger central value of the cross section at $\sqrt{S} = 5.5$ TeV in Table 1.

Thus the low x, low μ_F behavior of the gluon density depends strongly on how the group performing the global analysis chooses to extrapolate to unmeasured regions. All that is required is minimization of the global χ^2 and momentum conservation.

Since $0.5m_b \leq \mu_F \leq 2m_b$ lies well above both $\mu_0^{\rm CTEQ6M}$ and $\mu_0^{\rm GRV98}$, the factorization scale dependence of the gluon density at the bottom quark mass is not shown.

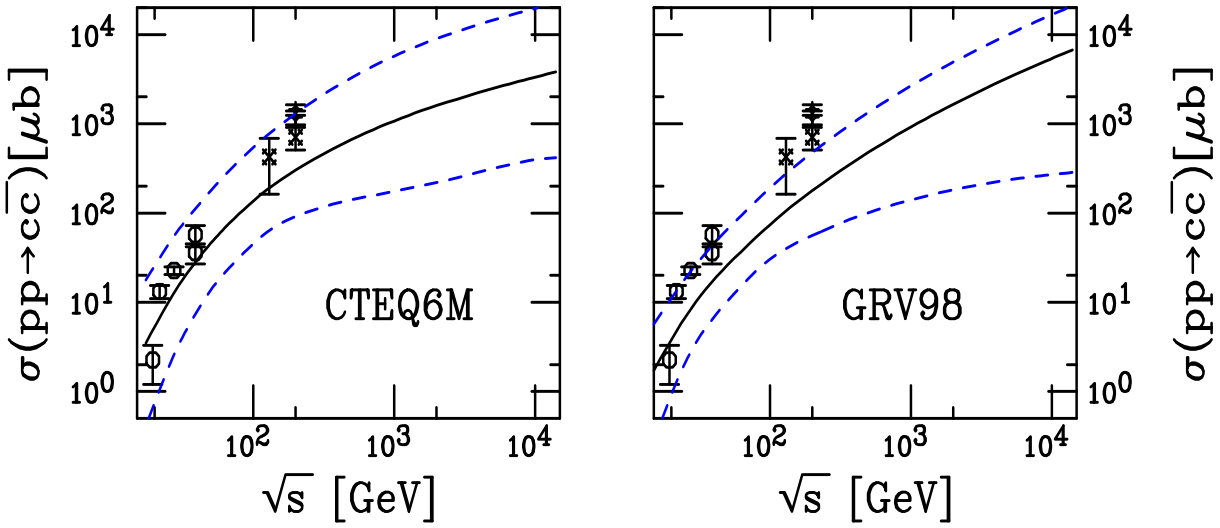

Fig. 1. The NLO total $c\bar{c}$ cross sections as a function of $\sqrt{S}$ for CTEQ6M (left-hand side) and GRV98 (right-hand side). The solid curve is the central result; the upper and lower dashed curves are the upper and lower edges of the uncertainty band.

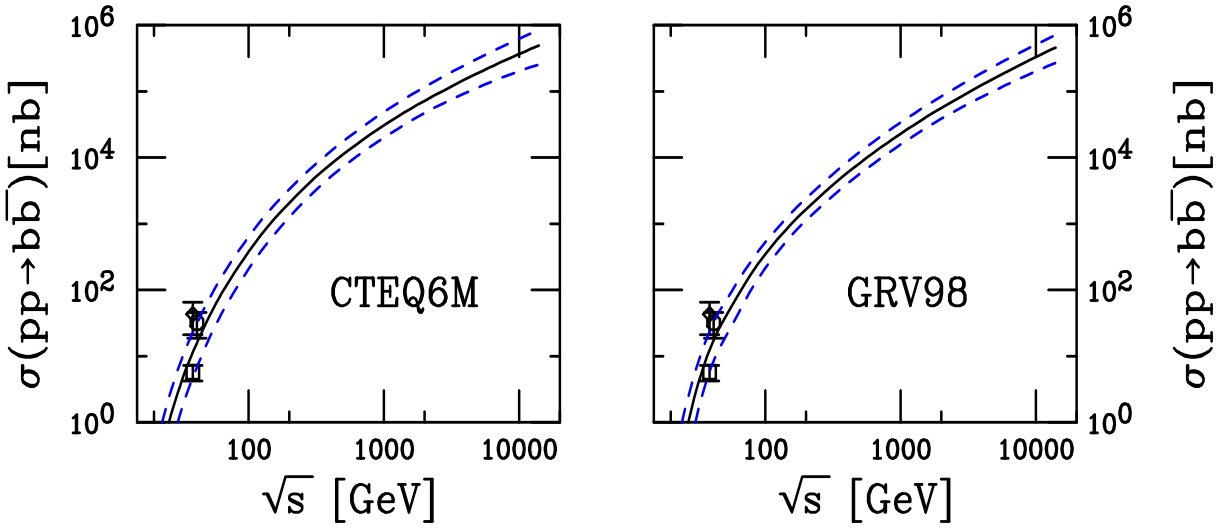

Fig. 2. The NLO total $b\bar{b}$ cross sections as a function of $\sqrt{S}$ for CTEQ6M (left-hand side) and GRV98 (right-hand side). The solid curve is the central result; the upper and lower dashed curves are the upper and lower edges of the uncertainty band.

Table 1. Summary of the uncertainty on the charm and bottom total cross sections calculated from the NLO partonic total cross sections at RHIC and the LHC.

	$\sqrt{S} = 200$ GeV			$\sqrt{S} = 5.5$ TeV	
Q	$\sigma^{\rm FONLL}_{\rm CTEQ6M}$ (μb)	$\sigma^{\rm NLO}_{\rm CTEQ6M}$ (μb)	$\sigma^{\rm NLO}_{\rm GRV98}$ (μb)	$\sigma^{\rm NLO}_{\rm CTEQ6M}$ (μb)	$\sigma^{\rm NLO}_{\rm GRV98}$ (μb)
c	256^{+400}_{-146}	301^{+1000}_{-210}	178^{+300}_{-122}	2585^{+13125}_{-2260}	3562^{+7321}_{-3321}
b	$1.87^{+0.99}_{-0.67}$	$2.06^{+1.25}_{-0.81}$	$1.65^{+0.77}_{-0.53}$	209^{+139}_{-84}	178^{+93}_{-64}

3.2 Renormalization and factorization scale dependence

As is obvious from Sec. 3.1, the smaller charm mass exaggerates the factorization scale dependence of the total cross section.

Thus the charm quark uncertainty band on the total cross section, Fig. 1, spans an order of magnitude at fixed-target energies, increasing to the value given in Tab: 1 for 200 GeV. The low scale behavior for $(\xi_R, \xi_F) = (0.5, 1)$ and (1,0.5) defines the upper and lower edges respectively of the uncertainty band at collider energies. Indeed, for the total cross section calculated with $n_{\rm lf}$ light quark flavors, the STAR point [12] is compatible with the upper limit of the band although the inclusive p_T data lies above the FONLL calculation with $n_{\rm lf}+1$ light flavors [16]. How-

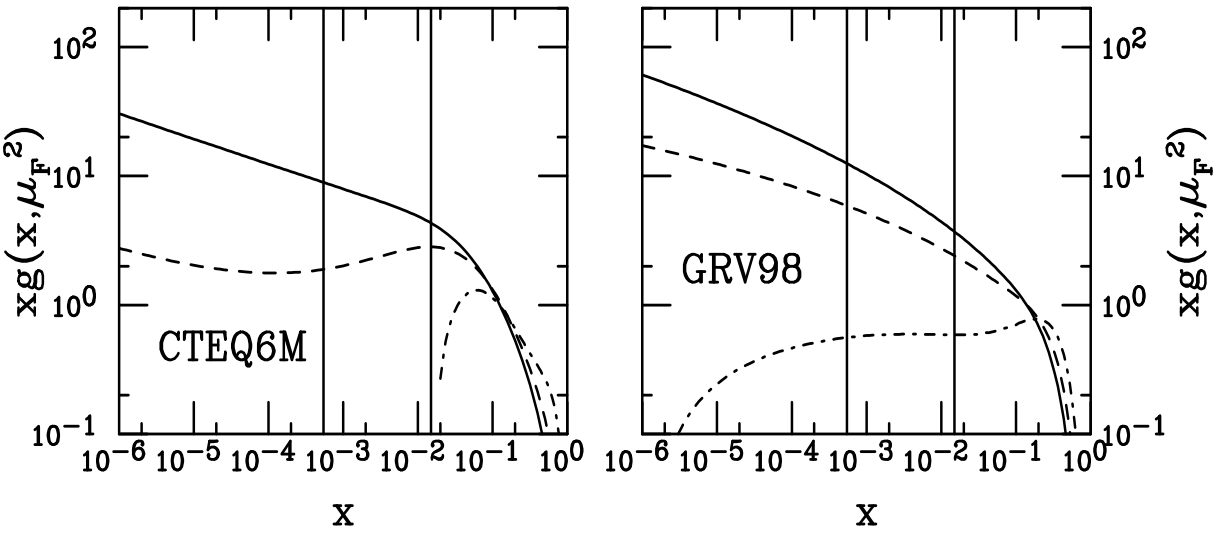

Fig. 3. The CTEQ6M (left) and GRV98 (right) gluon densities as a function of x for $\xi = 0.5$ (dot-dashed), $\xi = 1$ (dashed) and $\xi = 2$ (solid) for $m_c = 1.5$ GeV GeV. The vertical lines are at $x = 2m/\sqrt{S}$ in $\sqrt{S} = 200$ GeV and 5.5 TeV pp collisions at RHIC and the LHC.

ever, we stress that this apparent agreement of the STAR result with the total cross section does not mean that the discrepancy between the high p_T STAR results and the FONLL prediction is unimportant. At high p_T, the FONLL calculation is more reliable since here charm is correctly treated as an active flavor, with $n_{\rm lf}+1$, and light quark effects are resummed, improving the prediction at finite p_T.

The charm band grows broader with increasing $\sqrt{S}$, corresponding to decreasing x. Thus, without a better handle on the gluon density at low x and low scales, one may question whether such a large uncertainty is meaningful. It may also be questionable whether the lowest scales, μ_R, $\mu_F = 0.5m_c$ should be included in the calculation of the charm uncertainty, especially since $\mu_F < \mu_0$ for three light flavors.

The full fixed-target data set also exhibits a large uncertainty due to the method of extrapolation used, the assumed branching ratios and the A dependence [11]. However, if only the most recent data are used, as in Fig. 1, the uncertainty in the data is reduced. As an alternative, one may try to 'fit' the mass and scale parameters to these data [11] for $\mu_F, \mu_R > m$, obtaining $m_c = 1.2$ GeV with $\mu_F = \mu_R = 2m$ for CTEQ6M. In this case, the cross section lies just above the central value of the band and, although the quark mass is smaller than the assumed central mass value, the larger value of ξ_F guarantees a more regular $\sqrt{S}$ dependence than that obtained with smaller values.

The larger bottom quark mass ensures that the scale dependence is reduced and the uncertainty band is significantly narrower than for charm over the whole energy range, see Fig. 2.

For a more detailed discussion of the scale dependence of charm and bottom production, see Ref. [17].

3.3 The strong coupling constant and the number of light flavors

The most trivial difference in the FONLL and NLO calculations is that the FONLL p_T distribution is calculated with a running scale proportional to m_T while the total cross section is calculated with a fixed scale proportional to m. The charm quark uncertainty band is wider at low p_T, as shown in Ref. [5], because $p_T \leq m_c$. While it is more appropriate to use the running scale to calculate inclusive distributions, the difference between a fixed and a running scale can be checked by fixing the scale in the p_T distributions. The integral of the inclusive distribution increases about 20% for charm and about 10% for bottom when a fixed scale is used. This difference is approximately large enough to account for the difference in the central values of the total cross section.

The charm fiducial range, $0.5m_c \leq \mu_R \leq 2m_c$, is in a region where α_s is changing rapidly with μ_R. We can estimate the importance of the value of α_s to the uncertainty in the total cross section by looking at the dependence of α_s on the renormalization scale, shown in Table 2, with $\xi_R \equiv \mu_R/m$.

When calculated with the value of Λ_5 for CTEQ6M, $\Lambda_5 = 0.226$ GeV, and using a scheme where α_s is continuous across mass thresholds, we have the values of the two-loop α_s shown on the left-hand side of Table 2. The 3 and 4 light flavor values are calculated with masses appropriate for fixed-order (NLO) charm and bottom production respectively. It is clear that the charm uncertainty is larger than that for bottom since $\alpha_s(\xi_R = 0.5)/\alpha_s(\xi_R = 2) = 2.63$ for charm and 1.56 for bottom.

On the other hand, the faster evolution of the GRV98 PDFs, due to the lower initial scale, requires a smaller value of Λ_5, 0.1677 GeV. Thus even for relatively low μ_R, $\log(\mu_R/\Lambda)$ is larger, giving a lower α_s for GRV98, especially in the charm region, see the right-hand side of Ta-

Table 2. The values of α_s for charm and bottom production at the given values of $\xi_R = \mu_R/m$.

	CTEQ6M		GRV98	
ξ_R	$n_{\rm lf} = 3$, $m_c = 1.5$ GeV	$n_{\rm lf} = 4$, $m_b = 4.75$ GeV	$n_{\rm lf} = 3$, $m_c = 1.5$ GeV	$n_{\rm lf} = 4$, $m_b = 4.75$ GeV
0.5	0.6688	0.2822	0.3312	0.2183
1	0.3527	0.2166	0.2337	0.1781
2	0.2547	0.1804	0.1840	0.1511

ble 2. Now the ratio $\alpha_s(\xi_R = 0.5)/\alpha_s(\xi_R = 2) = 1.8$ for charm and 1.44 for bottom, contributing to the lower uncertainty range for this set.

The real difference in coupling strength between the two heavy quarks is even larger since the leading order cross section is proportional to α_s^2 while the next-order contribution is proportional to α_s^3.

One obvious contribution to the uncertainty is the difference in the number of flavors in the two calculations, especially for charm (3 for NLO and 4 for FONLL). Using $n_{\rm lf}+1$ in the FONLL and NLO calculations of the inclusive distributions reduces the uncertainty. When the FONLL total cross sections in Table 1 are instead calculated with $n_{\rm lf}$, the uncertainty is increased so that the upper and lower limits of the charm uncertainty are in agreement with the NLO results [18]. Thus whether charm is treated as a heavy ($n_{\rm lf}$) or an active ($n_{\rm lf}+1$) flavor in the calculation turns out to be one of the most important influences on the limits of the charm uncertainty.

4 Conclusions

We have shown that when the total cross section is calculated with the same parameter sets and the same number of light quark flavors, a consistent result is obtained by both integrating over an inclusive distribution and starting from the total partonic cross section, as should be expected. However, the charm results are extremely sensitive to the number of flavors, the scale choice and the parton densities. One of the biggest sources of uncertainty in the total charm cross section at collider energies is the behavior of the gluon density at low x and low scale, as yet not well determined, as evidenced by the large difference in the uncertainty band between the CTEQ6M and GRV98 PDFs. Until it is further under control, better limits on the charm quark total cross section will be difficult to set. A complete NNLO evaluation of the total cross section may reduce the scale dependence but will still be subject to the same types of uncertainties.

This work was performed under the auspices of the U.S. Department of Energy by Lawrence Livermore National Laboratory under Contract DE-AC52-07NA27344 and was also supported in part by the National Science Foundation Grant NSF PHY-0555660.

References

1. P. Nason, S. Dawson and R. K. Ellis, Nucl. Phys. B **303** (1988) 607; P. Nason, S. Dawson and R. K. Ellis, Nucl. Phys. B **327** (1989) 49 [Erratum-ibid. B **335** (1990) 260].
2. M. Cacciari, M. Greco and P. Nason, JHEP **9805** (1998) 007 [arXiv:hep-ph/9803400]; M. Cacciari, S. Frixione and P. Nason, JHEP **0103** (2001) 006 [arXiv:hep-ph/0102134].
3. W. Beenakker, W. L. van Neerven, R. Meng, G. A. Schuler and J. Smith, Nucl. Phys. B **351** (1991) 507.
4. M. Cacciari and M. Greco, Nucl. Phys. B **421** (1994) 530 [arXiv:hep-ph/9311260].
5. M. Cacciari, P. Nason and R. Vogt, Phys. Rev. Lett. **95** (2005) 122001 [arXiv:hep-ph/0502203].
6. N. Kidonakis, E. Laenen, S. Moch and R. Vogt, Phys. Rev. D **64** (2001) 114001 [arXiv:hep-ph/0105041].
7. N. Kidonakis, E. Laenen, S. Moch and R. Vogt, Phys. Rev. D **67** (2003) 074037 [arXiv:hep-ph/0212173].
8. N. Kidonakis and R. Vogt, Phys. Rev. D **68** (2003) 114014 [arXiv:hep-ph/0308222].
9. N. Kidonakis and R. Vogt, Eur. J. Phys. C **36** (2004) 201 [arXiv:hep-ph/0401056].
10. N. Kidonakis and R. Vogt, arXiv:0805.2844 [hep-ph].
11. R. Vogt [Hard Probe Collaboration], Int. J. Mod. Phys. E **12** (2003) 211 [arXiv:hep-ph/0111271].
12. J. Adams *et al.* [STAR Collaboration], Phys. Rev. Lett. **94** (2005) 062301 [arXiv:nucl-ex/0407006].
13. A. Adare *et al.* [PHENIX Collaboration], Phys. Rev. Lett. **97** (2006) 252002 [arXiv:hep-ex/0609010]; S. S. Adler *et al.* [PHENIX Collaboration], Phys. Rev. D **76** (2007) 092002 [arXiv:nucl-ex/0609032].
14. J. Pumplin *et al.*, *JHEP* **0207** (2002) 012 [arXiv:hep-ph/0201195]; D. Stump *et al.*, *JHEP* **0310** (2003) 046 [arXiv:hep-ph/0303013].
15. M. Glück, E. Reya and A. Vogt, *Eur. Phys. J.* C **5**, 461 (1998).
16. A. A. P. Suaide, J. Phys. G **34** (2007) 369 [arXiv:nucl-ex/0702035].
17. R. Vogt, Eur. Phys. J. Special Topics **155** (2008) 213 [arXiv:0709.2531 [hep-ph]].
18. M. Cacciari, private communication.